

Controlling Product Distribution of Polyethylene Hydrogenolysis Using Bimetallic RuM₃ (M = Fe, Co, Ni) Catalysts

Published as part of *Chem & Bio Engineering virtual special issue "Sustainable Catalysis"*.

Yong Yuan, Zhenhua Xie,* Kevin K. Turaczy, Sooyeon Hwang, Jiahua Zhou, and Jingguang G. Chen*



Cite This: *Chem Bio Eng.* 2024, 1, 67–75



Read Online

ACCESS |



Metrics & More



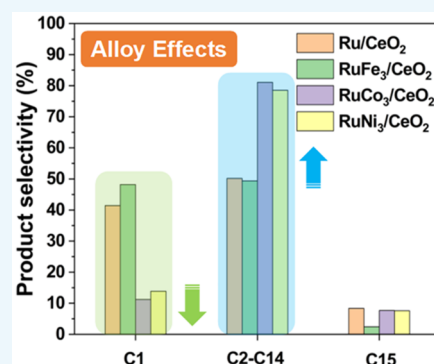
Article Recommendations



Supporting Information

ABSTRACT: Plastic hydrogenolysis is an attractive approach for producing value-added chemicals due to its mild reaction conditions, but controlling product distribution is challenging due to the formation of undesired CH₄. This work reports several bimetallic RuM₃/CeO₂ (M = Fe, Co, Ni) catalysts that shift the product of low-density polyethylene hydrogenolysis toward longer-chain hydrocarbons. These catalysts were characterized by using X-ray absorption fine structure spectroscopy, electron microscopy imaging, and H₂ temperature-programmed reduction. The combined catalytic evaluation and characterization results revealed that the product distribution was regulated by the formation of bimetallic alloys. A model compound, *n*-hexadecane, was selected to further understand the differences in hydrogenolysis over the Ru-based catalysts. Although a longer reaction time shifted the product toward smaller molecules, the bimetallic (RuCo₃/CeO₂) catalyst limited the further conversion of C₂–C₅ into CH₄. This work highlights the role of bimetallic alloys in tailoring the interaction with hydrocarbons, thereby controlling the product distribution of polymer hydrogenolysis.

KEYWORDS: Ru-based catalysts, Bimetallic catalysts, LDPE upgrading, *n*-Hexadecane conversion, Hydrocarbon adsorption



INTRODUCTION

Plastic upgrading has received growing attention due to the rapid increase in global plastic production and its non-biodegradable properties accompanied by environmental issues.^{1–3} Traditional solutions, such as landfill, incineration, and mechanical recycling, are often limited by the type of plastic.^{4–6} Chemical upcycling of plastic has been regarded as a potentially sustainable approach to achieving both the reduction of plastic waste and the production of value-added materials.^{7–9} Many chemical recycling technologies have been investigated, such as pyrolysis, solvolysis, hydrocracking, and hydrogenolysis,¹⁰ among which plastic hydrogenolysis has been widely investigated due to its relatively low reaction temperature, as well as an assortment of valuable products including gasoline, jet fuel, diesel, and lubricants.^{11–14}

Up until now, efforts on polymer hydrogenolysis have primarily focused on utilizing Ru or Pt monometallic catalysts as both types of catalysts have been shown to be capable of cleaving C–C bonds.¹⁵ Polymer hydrogenolysis over Pt catalysts typically occurs in the range 250–300 °C.^{16–18} Product distributions are centered on low molecular weight liquids, lubricants, and waxes. An acid zeolite support is typically used for Pt-catalyzed polymer hydrogenolysis and Brønsted acid density is leveraged to shift the carbon ranges of the products.¹⁹ Besides Pt, Ru has also been used for polymer hydrogenolysis in recent studies, with Ru/C being the most

widely studied.^{20–23} Typical reaction conditions require lower temperatures, 200–250 °C. While Ru is more active in alkane hydrogenolysis,¹⁵ it favors terminal C–C bond cleavage at low H₂ pressures, leading to poor selectivity toward value-added products.²⁰ There are, however, several factors that can vary the product distribution including reaction conditions (hydrogen pressure, reaction temperature, and reaction time) and catalyst design (electronic modification of the active species, support, and promoter impact).^{12,21,24,25} Wang et al.²⁶ demonstrated that by utilizing a WZrO₂ support, they could suppress the generation of CH₄, leading to more diesel- and liquid fuel-based products. Furthermore, the addition of effective dopant oxides (W, V, and Mo) could tune the product distribution for polyethylene hydrogenolysis by supplying hydrogen to Ru and facilitating the desorption of alkyl species.²⁷

Bimetallic catalysts have been investigated for the hydrogenolysis of low-density polyethylene (LDPE) as they can potentially improve the catalytic activity and selectivity

Received: August 26, 2023

Revised: November 20, 2023

Accepted: November 20, 2023

Published: January 4, 2024



compared to the corresponding monometallic catalysts.^{28–30} The synergistic interactions of bimetallic alloys often enhance the hydrogenolysis of LDPE by selectively promoting the cleavage of the internal C–C bonds in the polymer backbone and inhibiting the formation of gas products, such as methane and ethane.³¹ However, the optimization of the catalyst composition and control of product distribution to achieve maximum yield and selectivity toward desired products are still active areas of research.^{13,21,24,32–34} Thus far, Ru is among the most promising monometallic catalysts because of its high activity, although comparative studies incorporating different metals with Ru to form bimetallic catalysts have not been extensively explored for polymer hydrogenolysis.

In this work, bimetallic RuM₃/CeO₂ (M = Fe, Co, Ni) catalysts are shown to adjust the product distribution of LDPE hydrogenolysis at the expense of catalytic activity. The structural characterization of the investigated catalysts confirms the formation of the Ru–M alloy in the bimetallic catalysts, indicating that the presence of an alloy regulates the product distribution. Furthermore, using *n*-hexadecane as a model compound, the impact of reaction time and H₂ pressure was examined to gain insight into hydrogenolysis over the RuM₃/CeO₂ catalysts. Results from this study suggest that alloy formation weakens hydrocarbon adsorption, leading to a decrease in the catalytic activity while enhancing the product selectivity toward hydrocarbons with longer chains.

EXPERIMENTAL SECTION

Catalyst Preparation. All catalysts were synthesized via a slurry impregnation method, and all reagents were used without purification. For the synthesis of bimetallic catalysts, an appropriate amount of RuCl₃•H₂O (Sigma-Aldrich, 99.98% trace metals basis) was dissolved simultaneously with Fe(NO₃)₃•9H₂O (Sigma-Aldrich, ≥99.999% trace metals basis), Co(NO₃)₂•6H₂O (Sigma-Aldrich, 99.999% metal basis), or Ni(NO₃)₂•6H₂O (Alfa-Aesar, 99.9985% metal basis) in 30 mL of DI water to achieve a Ru/M ratio of 1:3. The slurry solution was subjected to ultrasonication for 10 min before adding the CeO₂ support (Sigma-Aldrich, 35–45 m² g^{−1}, <25 nm particle size (BET)) followed by another ultrasonication for 10 min. All the catalysts were dried at 80 °C overnight and then calcined at 400 °C for 2 h with a heating ramp rate of 1 °C/min. Following the same synthesis procedure, the monometallic catalysts were synthesized with the same metal loading as the corresponding bimetallic catalysts. The loadings of Ru and M (Fe, Co, Ni) were fixed to be 1.0% and 1.7%, respectively, which were confirmed by X-ray fluorescence spectroscopy (XRF) measurements, as summarized in Table S1. This loading corresponded to an atomic ratio of 1:3 (Ru:M). The Brunauer–Emmett–Teller (BET) surface areas of reduced Ru/CeO₂, RuFe₃/CeO₂, RuCo₃/CeO₂, and RuNi₃/CeO₂ were determined to be 35–37 m²/g (Figure S1).

Catalyst Characterization. The H₂ temperature-programmed reduction (H₂-TPR) profiles of the as-prepared catalysts were obtained by using an AMI-300ip (Altamira) instrument. Typically, ~100 mg of as-prepared catalyst was pretreated under Helium (He) atmosphere (50 mL/min) at 200 °C for 30 min and then cooled to 40 °C. TPR measurements were subsequently performed in a mixture of 10% H₂/Ar (30 mL/min total) with a heating rate of 10 °C/min to 800 °C. Pulse CO chemisorption was performed in an AMI-300ip (Altamira) instrument.³⁵ The as-prepared catalyst (~100 mg) was prerduced at elevated temperatures (Co- and Ni-related samples were reduced at 400 °C, Fe-related samples were reduced at 600 °C, and monometallic Ru was reduced at 200 °C) for 60 min under 10% H₂/Ar (30 mL/min total), and cooled down to 40 °C in He (50 mL/min), before periodically pulsing 10% CO/He (590 μL loop) into the pretreated catalysts. Elemental analysis was performed by XRF (Rigaku WDXRF). Ru-based samples were degassed overnight at 250 °C after which the BET surface area was determined using N₂

adsorption isotherms (−196 °C) on a Micromeritics 3Flex system. Electron microscopy characterization of the reduced and spent catalysts was performed at the Center for Functional Nanomaterials at Brookhaven National Laboratory. For these measurements, samples were ultrasonically dispersed in ethanol for 10 min, and then a droplet of the dispersed sample was placed onto a Lacey carbon film supported by a copper grid and allowed to dry thoroughly. Transmission electron microscopy (TEM) images were captured using a JEOL 1400 instrument and a Thermo-Fisher Talos F200X. To determine the elemental distribution of the spent Ru-based monometallic and bimetallic catalysts, high-angle annular dark-field scanning transmission electron microscopy (HAADF-STEM) images and energy dispersive X-ray spectroscopy (EDS) elemental maps were obtained with a Thermo-Fisher Talos F200X at an accelerating voltage of 200 kV.

The ex-situ X-ray absorption fine structure (XAFS) spectra of the Ru K-edge were collected at beamline 7-BM (QAS) of the National Synchrotron Light Source II (NSLS-II) at Brookhaven National Laboratory. For each measurement, the spent catalyst was pressed and sealed with Kapton tape. The XAFS spectra were recorded simultaneously via transmission and fluorescence modes. Ru foil was applied as the standard reference to calibrate energy shift as well as to obtain the passive electron reduction factor (S₀²) used for fitting. Data processing was performed using the IFEFFIT package.³⁶

Hydrogenolysis Reactions and Product Quantification. LDPE and *n*-Hexadecane Hydrogenolysis Reactions. Before the batch reactions, RuM₃/CeO₂ and M₃/CeO₂ (M = Fe, Co, Ni) catalysts were reduced in a tube furnace by a 50 vol % H₂/Ar flow at elevated temperatures for 60 min with a ramp rate of 10 °C/min, with the reduction temperature being determined via H₂-TPR profiles, similar to those described for CO chemisorption experiments. There was no prerduction process for Ru/CeO₂ since Ru could be fully reduced below the reaction temperature (250 °C). Afterward, the reduced sample was cooled down in Ar to room temperature and passivated by 1 vol % O₂/Ar for 15 min before being transferred to the batch reactor, a 4598 Parr micro stirred reactor. For each measurement, 10–200 mg of the reduced catalyst was loaded into a small beaker and mixed with 1 g of reactant (LDPE with M_w ~ 4000 Da or *n*-hexadecane) before being added to a 100 mL stainless steel autoclave. The reactor was tightly sealed and purged with H₂ (18 bar) six times prior to being filled to the target H₂ pressure (5 or 18 bar). The reactor was heated to reaction temperature (200 or 250 °C) in 40 min, maintained at the reaction temperature for a specific time (30–600 min) under agitation, and then cooled down to room temperature before collecting gases, liquids, and solid residues for product analysis.

Product Analysis and Quantification. After the reactor cooled to room temperature, the gas products were slowly released into a 2 L jumbo syringe until the mixture reached ambient pressure. Following gas product collection, 15 mL of acetylene was injected into the syringe as an internal standard and mixed with the gas products. The gaseous mixture was pushed into and analyzed by an Agilent 7890B gas chromatograph (GC) (PLOT Q and MOLESEIVE columns) equipped with a thermal conductivity detector (TCD) and a flame ionized detector (FID). To avoid any condensation of high-boiling-point products, the gas line from the jumbo syringe to the GC inlet was wrapped in heating tape and maintained at 150 °C.

Dichloromethane (CH₂Cl₂, Sigma-Aldrich, ≥99.9%) was used to extract soluble products from LDPE or *n*-hexadecane conversion, denoted as liquid products, which consisted of C₄–C₃₀ from LDPE conversion and C₄–C₁₅ from *n*-hexadecane conversion. Following liquid product collection, 50 μL of *n*-butylcyclohexane was employed as an internal standard. The liquid product was analyzed by another Agilent 7890B GC instrument equipped with an FID and an HP-5 column. For quantification, the FID response factors of all of the gaseous and liquid products were obtained from calibration with standards.

The yield and selectivity of the product was calculated on a per-carbon basis, with *i* carbons (C_{*i*}), using the following equation:

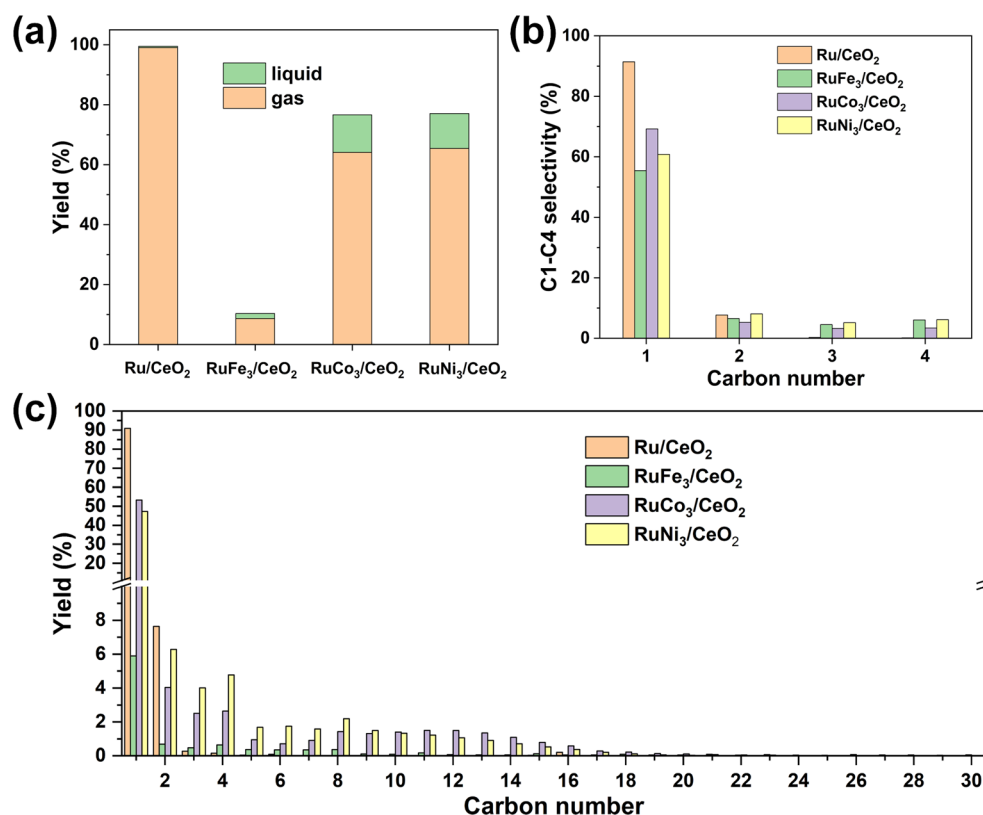


Figure 1. Effect of different bimetallic $\text{RuM}_3/\text{CeO}_2$ ($M = \text{Fe}, \text{Co}, \text{Ni}$) catalysts on LDPE hydrogenolysis. (a) Yield of gas and liquid products, (b) selectivity of light molecules (C1–C4), and (c) carbon distributions of C1–C30 products. Reaction conditions: 100 mg of catalyst, 1 g of LDPE, 250 °C, 18 bar of H_2 , 600 min.

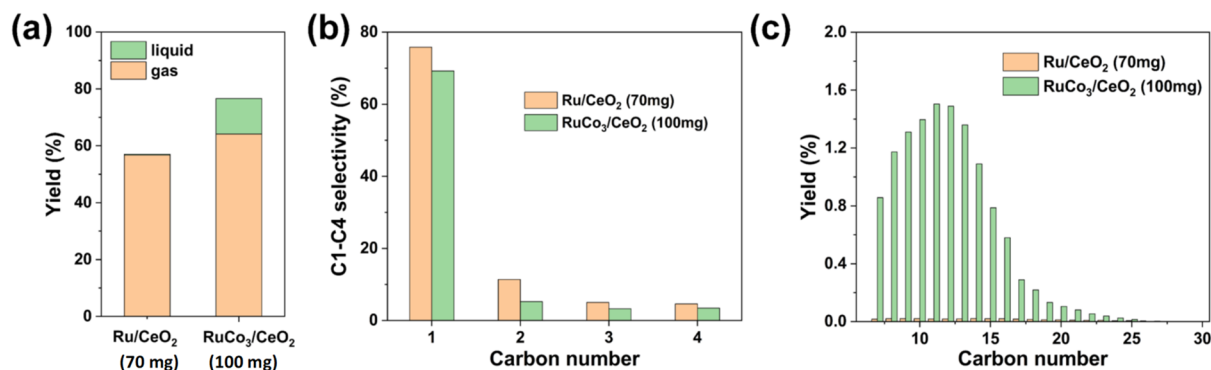


Figure 2. Product distributions of LDPE hydrogenolysis on Ru/CeO_2 and $\text{RuCo}_3/\text{CeO}_2$ catalysts at comparable conversions. (a) Yield of gas and liquid products, (b) selectivity of light molecules (C1–C4), and (c) distributions of C6–C30 products. Reaction conditions: 1 g of LDPE, 250 °C, 18 bar of H_2 , 600 min.

$$\text{Yield} = \left(\frac{n_{i,\text{product}}}{n_{\text{reactant}}} \right) \times 100\% \quad (1)$$

$$\text{Selectivity} = \frac{n_{i,\text{product}}}{\sum n_{i,\text{product}}} \times 100\% \quad (2)$$

where i represents the carbon number of alkane products, n_i is the number of carbon atoms of component i , and n_{reactant} is the total number of carbon atoms of the reactant (LDPE or n -hexadecane).

RESULTS AND DISCUSSION

Bimetallic Effects on LDPE Hydrogenolysis. LDPE with a M_w of ~ 4000 Da was selected to investigate the impact of bimetallic formation on the hydrogenolysis product distribu-

tion. As illustrated in Figure 1, Ru/CeO_2 showed near 100% LDPE conversion, with primarily gaseous products, consisting of $\sim 90\%$ CH_4 with a small amount of C_2H_6 . This is consistent with reported results that Ru-based catalysts favor C–C bond scission of polymers in the presence of H_2 leading to the production of CH_4 .¹³ It is noteworthy that different product distributions of polymer hydrogenolysis on Ru/CeO_2 have also been reported. Nakaji et al.³⁷ found that Ru/CeO_2 (5 wt % Ru) could achieve 92% yield of liquid fuel and wax at 200 °C with H_2 pressure of 20 bar. However, a more recent study by Chen et al.¹³ pointed out that the product distribution for polymer hydrogenolysis over Ru/CeO_2 was dependent on the Ru loading with a high Ru loading (>0.5 wt %) favoring CH_4 formation. Many factors, such as reaction temperature, H_2

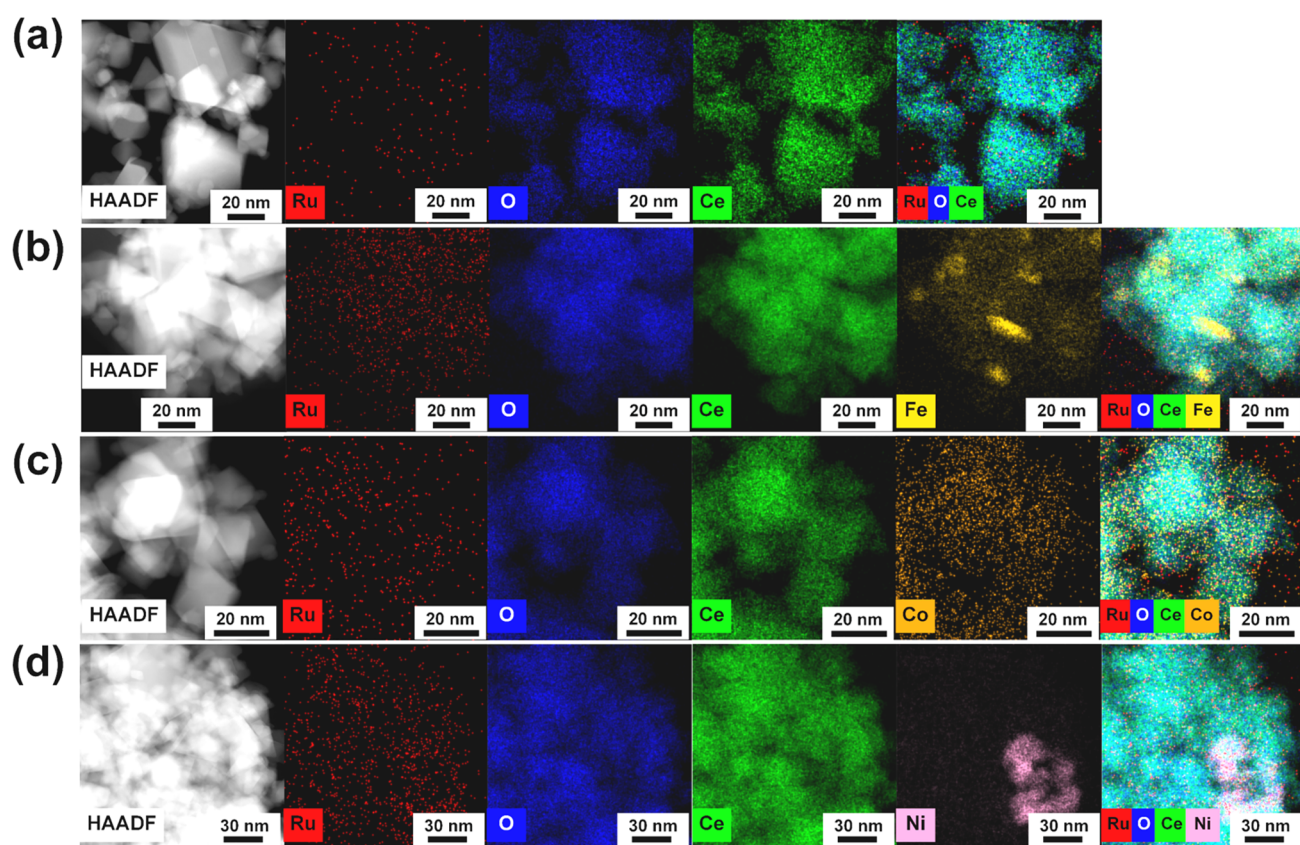


Figure 3. HAADF-STEM image and corresponding STEM-EDS image of the spent (a) Ru/CeO₂, (b) RuFe₃/CeO₂, (c) RuCo₃/CeO₂, and (d) RuNi₃/CeO₂ catalysts.

pressure, the ratio of catalyst to reactant, particle size of the active species, etc., could impact the product distribution for polymer hydrogenolysis.^{13,24,26,32} Following the addition of a second metal (Fe, Co, Ni) to the Ru/CeO₂ catalyst, the reactivity of LDPE conversion decreased compared to that of Ru/CeO₂ (Figure 1a). Both RuCo₃/CeO₂ and RuNi₃/CeO₂ delivered ~80% LDPE conversion, while the conversion for RuFe₃/CeO₂ was notably lower. Interestingly, a fraction of liquid products was obtained over all bimetallic RuM₃/CeO₂ catalysts, indicating that the addition of a second metal could tailor the product distribution of LDPE hydrogenolysis. The CH₄ selectivity decreased from ~90% on Ru/CeO₂ to ~70% on RuM₃/CeO₂, while the C₂–C₄ selectivity remained almost unchanged (Figure 1b). RuCo₃/CeO₂ and RuNi₃/CeO₂ showed appreciable amounts of products between C₅–C₁₆ (Figure 1c and Figure S2), which could be potentially used in gasoline and jet fuels.²⁶

Considering that the product distribution of LDPE hydrogenolysis should be dependent on the conversion, the products of Ru/CeO₂ and RuCo₃/CeO₂ were compared at similar LDPE conversions. As shown in Figure 2a, negligible amounts of liquid products were observed, even though a lower LDPE conversion was obtained by decreasing the amount of Ru/CeO₂ used (70 mg). Although the CH₄ selectivity decreased from ~90% at complete LDPE conversion to ~77% at 60% LDPE conversion, lower alkanes, primarily ethane and propane, made up the remainder of the products (Figure 2b). Therefore, bimetallic RuCo₃/CeO₂ catalyst could adjust the product distribution of LDPE hydrogenolysis toward hydrocarbons with longer chains.

Structural Characterization. High-angle annular dark field (HAADF) and scanning transmission electron microscopy with energy dispersive spectroscopy (STEM-EDS) images were collected on the spent Ru/CeO₂ and RuM₃/CeO₂ (M = Fe, Co, Ni) catalysts, as shown in Figure 3. For all samples (Figure 3a–d), Ru was uniformly distributed on the CeO₂ support. Importantly, Co was also found to be distributed evenly on the spent RuCo₃/CeO₂ catalyst (Figure 3c), suggesting possible interactions between Ru and Co, likely the formation of a RuCo alloy in the RuCo₃/CeO₂ catalyst. Unlike Co, Fe and Ni aggregated in RuFe₃/CeO₂ and RuNi₃/CeO₂, respectively (Figure 3b,d), suggesting that the fraction of Ru–Co alloy formation should be higher than those of the Ru–Fe and Ru–Ni alloys. Note that Ru nanoparticles could not be easily discerned from the CeO₂ support due to the high atomic number of Ce. The TEM measurements of the reduced Ru-based catalysts were also attempted, considering that potential hydrocarbon species deposition on the spent catalyst might obscure the distinct visualization of Ru nanoparticles. As shown in Figure S3, Ru nanoparticles were still not easily discernible from the CeO₂ support, given the diameter of the support was below 25 nm. Therefore, the average coordination numbers (CNs) of the total Ru–M bonds (see Table S3) obtained from the extended X-ray absorption fine structure (EXAFS) analysis were utilized to estimate the average Ru-relevant particle size. Assuming a hemispherical shape, the average CN in the first coordination shell approximated similar average sizes (3–5 nm) over the Ru/CeO₂ and RuM₃/CeO₂ catalysts, which allowed for meaningful comparisons of selectivity in the context of alloy formation.

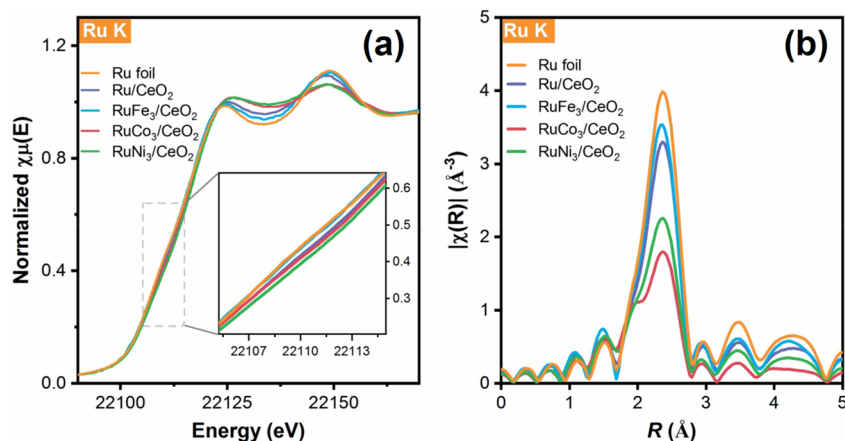


Figure 4. Ex-situ XAFS spectra of Ru K-edge over the spent Ru/CeO₂, RuFe₃/CeO₂, RuCo₃/CeO₂, and RuNi₃/CeO₂ catalysts, as well as the Ru foil. (a) XANES spectra and (b) Fourier transform (FT)-EXAFS spectra in R space. The inset indicates the amplified region around the edge position.

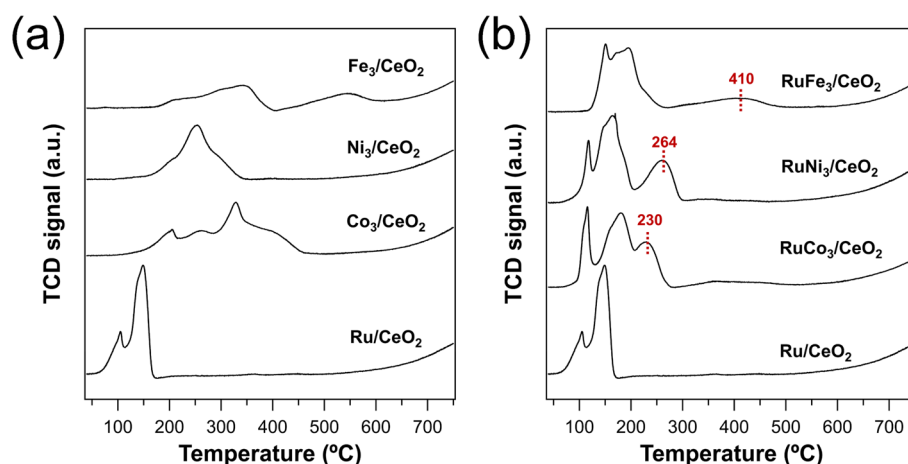


Figure 5. H₂-TPR profiles of (a) monometallic and (b) Ru-based bimetallic catalyst.

To probe the chemical state and local coordination environment of Ru, the X-ray absorption near edge structure (XANES) and EXAFS spectra were measured for the CeO₂ supported Ru-based monometallic and bimetallic catalysts after the LDPE conversion as well as for the Ru foils. Both CN and bond distance (d) were determined from EXAFS fittings. As shown in Figure 4, the XANES region of the Ru K-edge indicated a predominantly metallic feature compared to that of the Ru foil. The RuCo₃/CeO₂ and RuNi₃/CeO₂ samples exhibited a slightly higher edge position and white line intensity in addition to a broad resonance shape due to the orbital hybridization between Ru and Co or Ni.^{38,39} Indeed, the EXAFS fitting at the Ru K-edge indicated the formation of a Ru–Co ($CN_{Ru-Co} = 2.5 \pm 0.5$, $d_{Ru-Co} = 2.57$ Å) or Ru–Ni ($CN_{Ru-Ni} = 1.4 \pm 0.5$, $d_{Ru-Ni} = 2.54$ Å) bond, in addition to the Ru–Ru bond (RuCo₃/CeO₂: $CN_{Ru-Ru} = 8.1 \pm 0.7$, $d_{Ru-Ru} = 2.65$ Å; RuNi₃/CeO₂: $CN_{Ru-Ru} = 8.0 \pm 0.6$, $d_{Ru-Ru} = 2.66$ Å), consistent with the doublet peaks in the FT-EXAFS plots. Given their higher selectivity of liquid products compared to Ru/CeO₂ at similar LDPE conversions, alloy formation should be responsible for modifying the selectivity for LDPE hydrogenolysis. Both the Ru/CeO₂ and RuFe₃/CeO₂ samples showed a very similar edge position (see the inset in Figure 4a) and resonance character to those of the Ru foil, consistent with their similar FT-EXAFS peak feature in the R space (Figure

4b). Accordingly, only the Ru–Ru bond was obtained from the EXAFS fitting, as indicated by the coordination number and the bond distance in Table S3 (Ru/CeO₂: $CN_{Ru-Ru} = 10.5 \pm 0.3$, $d_{Ru-Ru} = 2.68$ Å; RuFe₃/CeO₂: $CN_{Ru-Ru} = 10.3 \pm 1.1$, $d_{Ru-Ru} = 2.67$ Å). Thus, Ru in the RuFe₃/CeO₂ catalyst should reside in a similar chemical state and coordination environment as that of the Ru/CeO₂ catalyst. The RuFe₃/CeO₂ catalyst, however, was nearly inactive toward LDPE conversion, much lower than the Ru/CeO₂ catalyst. Moreover, the HAADF and EDS imaging (Figure 3b) showed that the Fe species generally overlapped with Ru, despite some heterogeneity. It is hypothesized that the Ru sites were partially encapsulated or shielded by FeO_x species, which would prevent the access of LDPE molecules to the Ru sites, thus leading to low reactivity. This can be further supported by the negligible amount of CO chemisorption over the RuFe₃/CeO₂ catalyst (Table S2). Chen et al.³⁰ also found that in the case of polyethylene conversion over Fe-doped Pt/Al₂O₃ catalysts, Fe species covered the Pt sites when Fe/Pt ratios reached 1, resulting in the deactivation of catalytic activity.

The H₂-TPR experiments provided additional information on the reduction properties of the monometallic and bimetallic catalysts (Figure 5). Ru/CeO₂ showed a low reduction temperature below 200 °C (Figure 5a). Ni₃/CeO₂ was characterized by a broad reduction peak between 200 and

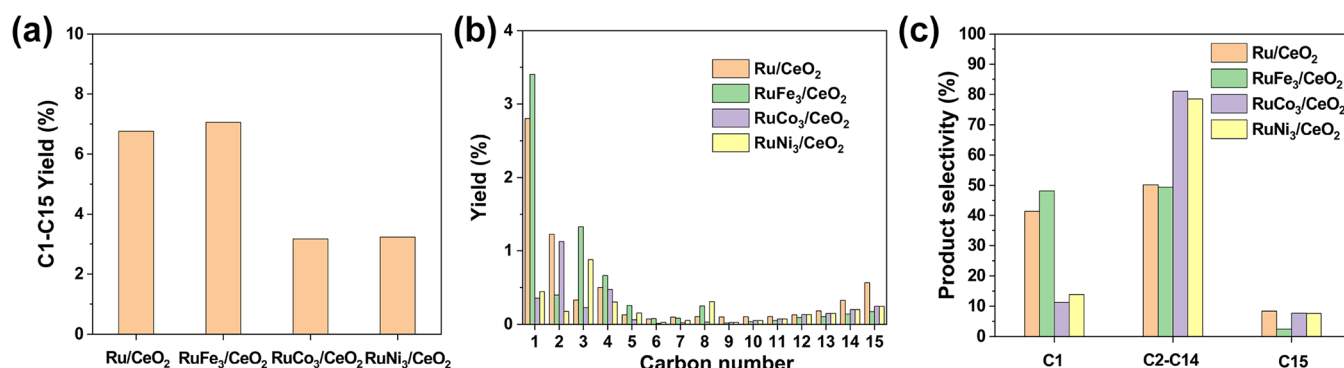


Figure 6. Comparison of monometallic and bimetallic RuM₃/CeO₂ (M = Fe, Co, Ni) catalysts for *n*-hexadecane hydrogenolysis under comparable conversions (3–7%). (a) Yield of all products, (b) Yield of each product, and (c) product selectivity. Reaction conditions: 10–200 mg catalyst, 1 g of *n*-hexadecane, 200 °C, 18 bar H₂, 30 min.

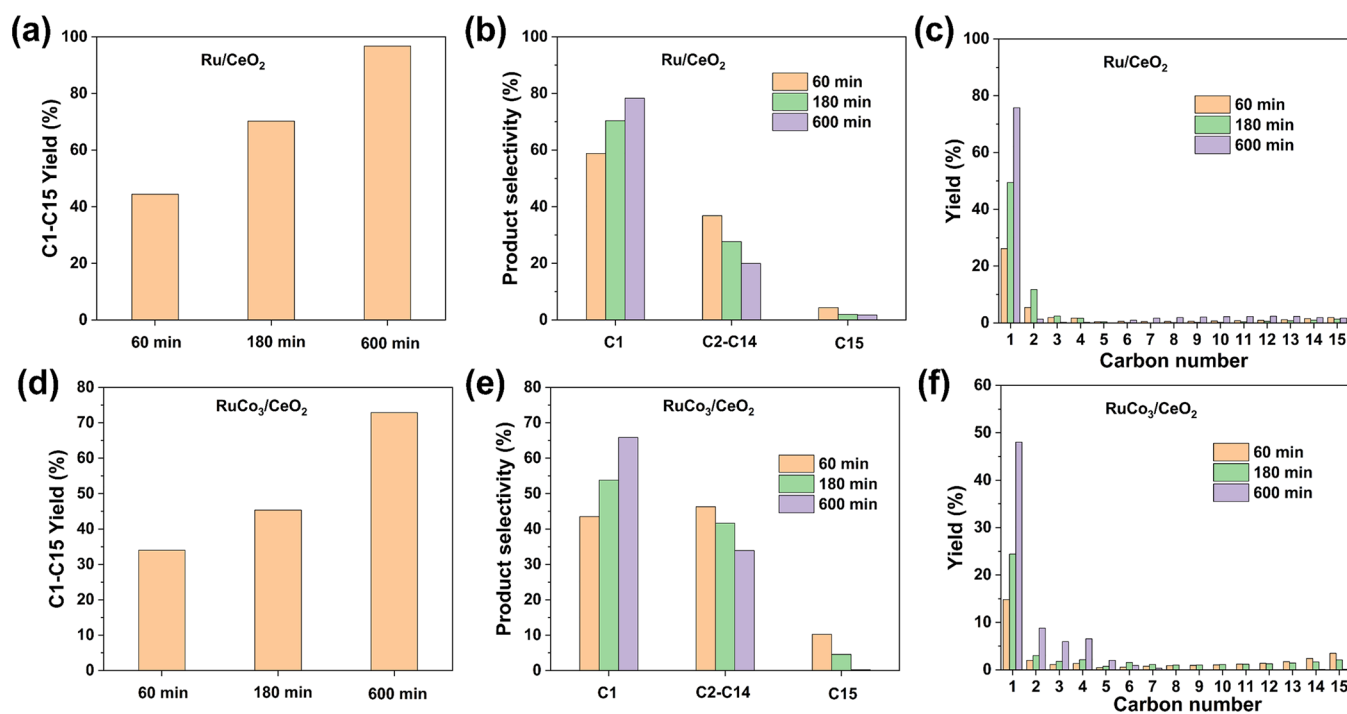


Figure 7. Impact of reaction time on *n*-hexadecane hydrogenolysis over Ru/CeO₂ and RuCo₃/CeO₂ catalysts. (a) Yield, (b) selectivity, and (c) product distribution of *n*-hexadecane hydrogenolysis on Ru/CeO₂ with different reaction times. (d) Yield, (e) selectivity, and (f) product distribution of *n*-hexadecane hydrogenolysis on RuCo₃/CeO₂ with different reaction times. Reaction conditions: 100 mg of catalyst, 1 g of *n*-hexadecane, 250 °C, 18 bar H₂.

350 °C with the center at 250 °C, representing the reduction of NiO to metallic Ni.⁴⁰ Several reduction peaks were observed on both Fe₃/CeO₂ and Co₃/CeO₂ samples, due to the presence of multiple oxidation states and phases during the reduction, such as M₂O₃, M₃O₄, MO, and M (M = Fe and Co).⁴¹ Between the two samples, Co₃/CeO₂ showed an easier reduction than Fe₃/CeO₂ since the former underwent a complete reduction below 450 °C, while Fe₃/CeO₂ was not fully reduced until 600 °C. Note that H₂ consumption at temperatures above 650 °C was due to the reduction of the CeO₂ support.^{32,42} Compared to monometallic M₃/CeO₂ (M = Fe, Co, Ni), bimetallic RuM₃/CeO₂ showed a lower reduction temperature due to the promoted reduction effect of Ru (Figure 5b). The reduction temperature was the lowest for RuCo₃/CeO₂, followed by those of RuNi₃/CeO₂ and RuFe₃/CeO₂. The prominent decrease in the reduction temperature was likely related to the close interaction between

Ru and the metal oxides, MO_x, leading to an easier reduction of the MO_x. This was consistent with the XAFS results where a higher fraction of Ru–M alloy was observed in RuCo₃/CeO₂ than in RuNi₃/CeO₂ and RuFe₃/CeO₂.

Overall, the combined structural characterizations indicate that Ru–M alloys are formed in reduced RuM₃/CeO₂ catalysts with RuCo₃/CeO₂ forming the highest fraction of Ru–M alloys among the three bimetallic catalysts. Together with the LDPE hydrogenolysis performance, it can be seen that the formation of the Ru–M alloy plays an important role in regulating the product distribution of LDPE hydrogenolysis.

Mechanistic Insights. Considering that many factors impact the performance of LDPE hydrogenolysis, such as mass transfer and the ability of large molecules/intermediates to adsorb on the catalyst surface, *n*-hexadecane was selected as a model compound to facilitate the mechanistic understanding of the effect of utilizing bimetallic catalysts for hydro-

genolysis.^{25,27} In a comparison of several monometallic catalysts (Figure S4a), Ru/CeO₂ showed the highest conversion of *n*-hexadecane, followed by Co₃/CeO₂, Fe₃/CeO₂, and Ni₃/CeO₂. Similar to LDPE hydrogenolysis, Ru/CeO₂ favored the formation of CH₄ (~80%) from the terminal C–C bond break (Figure S4b,c). In contrast, Co₃/CeO₂ and Ni₃/CeO₂ showed ~40% CH₄ selectivity, with ~40% selectivity toward C2–C14 products from the internal C–C bond cleavage of *n*-hexadecane, indicating a lack of preference for the terminal and internal C–C bond scission. Interestingly, Fe₃/CeO₂ demonstrated a preference for internal C–C bond cleavage. However, the low hydrogenolysis activity of Fe₃/CeO₂ and Ni₃/CeO₂ makes them less likely to compete with the more widely investigated Ru-based catalysts.

The *n*-hexadecane hydrogenolysis on bimetallic RuM₃/CeO₂ provided additional insights into the role of the second metal (Figure S4d–f). Overall, the addition of the second metal decreased the catalytic activity compared to Ru/CeO₂. RuCo₃/CeO₂ and RuNi₃/CeO₂ catalysts showed comparable *n*-hexadecane conversion, with both being more active than RuFe₃/CeO₂ (Figure S4d). More importantly, the three bimetallic RuM₃/CeO₂ catalysts showed a lower CH₄ yield and selectivity (Figure S4e,f). The catalyst loading was changed in order to compare the product selectivity of *n*-hexadecane hydrogenolysis over Ru/CeO₂ and RuCo₃/CeO₂ under comparable conversions (Figure S5), and the results confirmed that RuCo₃/CeO₂ showed a lower CH₄ selectivity than Ru/CeO₂. Considering that the measured *n*-hexadecane conversions (>50%) were relatively high due to the high reaction temperature (250 °C) and extended reaction time (600 min), such a prolonged duration could drive the hydrogenolysis of both the reaction intermediates and the final products, favoring methane formation. In light of this, the *n*-hexadecane hydrogenolysis was measured under comparably low conversions (3–7%) at a lower reaction temperature (200 °C) and a shorter reaction time (30 min). As illustrated in Figure 6, at a comparable conversion (3–7%), the RuCo₃/CeO₂ and RuNi₃/CeO₂ catalysts exhibited 10% methane selectivity. This was significantly lower than that observed for the Ru/CeO₂ and RuFe₃/CeO₂ catalysts (~40%). These catalytic activities and selectivity trends are generally consistent with the performance of LDPE hydrogenolysis, indicating that the Ru–M alloy favors internal C–C bond scission, which is significantly different from that of the Ru monometallic catalyst.

The impact of reaction time (Figure 7) and H₂ pressure (Figure S6) on the catalytic activity and product distribution of *n*-hexadecane hydrogenolysis was also examined over the Ru/CeO₂ and RuCo₃/CeO₂ catalysts. As expected, the *n*-hexadecane conversion increased with the reaction time (Figure 7a,d). Meanwhile, the CH₄ selectivity grew with the reaction time (Figure 7b,e), likely due to the subsequent adsorption and hydrogenolysis of the product to form CH₄. This is consistent with the general trends that the products of alkane hydrogenolysis shift to shorter-chain hydrocarbons with increasing reaction time.^{21,26} Interestingly, for Ru/CeO₂, at the initial stage (60 min) (Figure 7c), the product was dominated by CH₄ with a small fraction of C₂H₆. As the reaction time progressed to 180 min, more CH₄ and C₂H₆ were produced without the significant formation of C3–C15. A longer reaction time led to an increase in CH₄ yield and a decrease in C₂H₆ yield, suggesting that Ru/CeO₂ was active toward adsorption and C–C bond scission even for small molecules,

such as C₂H₆ and C₃H₈. A different trend was observed for the RuCo₃/CeO₂ catalyst (Figure 7f). As the reaction time progressed, the yield of light alkanes (C1–C5) grew continuously, while the yield of medium alkanes (C6–C8) increased first in the initial stage and then decreased after a longer reaction time. The continuous increase of the C1–C5 yield suggested that these molecules did not undergo further hydrogenolysis once formed. The different product distribution between Ru/CeO₂ and RuCo₃/CeO₂ is likely from their intrinsic ability for hydrocarbon adsorption and hydrogenolysis—Ru species could continuously adsorb alkanes (C_{*n*}H_{2*n*+2}, *n* ≥ 2) and eventually convert them to CH₄, leading to a high CH₄ selectivity, while Ru–Co alloy continuously catalyzes alkane (C_{*n*}H_{2*n*+2}, *n* ≥ 6) hydrogenolysis, though lower alkanes were not further converted to CH₄.

The influence of H₂ pressure on *n*-hexadecane hydrogenolysis was investigated by using the RuCo₃/CeO₂ catalyst. As shown in Figure S6, at low *n*-hexadecane and H₂ conversions (below 20%), an increase in H₂ pressure from 5 to 18 bar resulted in a decrease in the overall yield of all products. This was likely due to the increased hydrogen coverage on the catalyst surface, which inhibited the activity.²⁷ Notably, the product distribution remained relatively unchanged. Consequently, the effect of H₂ pressure on the product distribution was considered negligible on the selected H₂ pressure ranges.²⁷ Therefore, although the RuCo₃/CeO₂ catalyst showed a decrease in the hydrogenolysis activity of both LDPE and *n*-hexadecane compared to Ru/CeO₂, the alloy protects the subsequent hydrogenolysis of small molecules and thus decreases the selectivity of CH₄. This observation is consistent with trends identified from previous experimental and theoretical studies of bimetallic surfaces containing a Pt-group metal and a 3rd-row transition metal such as Fe, Co, or Ni;⁴³ in the presence of H₂, these bimetallic surfaces typically bond to hydrocarbon species more weakly than either of the parent metal surfaces alone.

CONCLUSIONS

In summary, the current paper reports the hydrogenolysis of *n*-hexadecane and LDPE over monometallic and bimetallic RuM₃/CeO₂ (M = Fe, Co, or Ni) catalysts. Unlike the product distribution of Ru/CeO₂, which is dominated by CH₄ formation, the addition of a second metal (Fe, Co, Ni) to Ru/CeO₂ modifies the product distribution to produce hydrocarbons with longer chains. Among the three RuM₃/CeO₂ catalysts, Co shows a better promotion effect due to the greater extent of alloy formation, which plays an important role in tailoring the product distribution from LDPE hydrogenolysis. The utilization of *n*-hexadecane as a model compound provides a further understanding of the effects of reaction time and H₂ pressure. The results show that longer reaction time shifts the product distribution toward short-chain molecules. The lower alkanes (C2–C5) can be further converted to CH₄ on Ru/CeO₂, while they are not on RuCo₃/CeO₂. This suggests that alloy formation weakens hydrocarbon adsorption, resulting in a decrease in hydrogenolysis activity but regulates the product distribution to hydrocarbons with longer chains. These results highlight the importance of bimetallic alloys in controlling the activity and product selectivity for polymer hydrogenolysis.

■ ASSOCIATED CONTENT

SI Supporting Information

The Supporting Information is available free of charge at <https://pubs.acs.org/doi/10.1021/cbe.3c00007>.

N₂ adsorption–desorption isotherms of the reduced catalysts, catalyst impact on LDPE hydrogenolysis, TEM images, catalyst comparison and product distribution for *n*-hexadecane hydrogenolysis, and impact of H₂ pressure on *n*-hexadecane hydrogenolysis, tables of active metal loading, CO uptakes, and EXAFS fitting results (PDF)

■ AUTHOR INFORMATION

Corresponding Authors

Zhenhua Xie – Department of Chemical Engineering, Columbia University, New York, New York 10027, United States; orcid.org/0000-0003-3737-8894; Email: zhenhuaxie369@gmail.com

Jingguang G. Chen – Chemistry Division, Brookhaven National Laboratory, Upton, New York 11973, United States; Department of Chemical Engineering, Columbia University, New York, New York 10027, United States; orcid.org/0000-0002-9592-2635; Email: jgchen@columbia.edu

Authors

Yong Yuan – Chemistry Division, Brookhaven National Laboratory, Upton, New York 11973, United States

Kevin K. Turaczy – Department of Chemical Engineering, Columbia University, New York, New York 10027, United States

Sooyeon Hwang – Center for Functional Nanomaterials, Brookhaven National Laboratory, Upton, New York 11973, United States; orcid.org/0000-0001-5606-6728

Jiahua Zhou – Department of Chemical and Biomolecular Engineering, University of Delaware, Newark, Delaware 19716, United States

Complete contact information is available at:

<https://pubs.acs.org/10.1021/cbe.3c00007>

Author Contributions

Y.Y. and Z.X. contributed equally. The manuscript was written through the contributions of all authors. All authors have given approval to the final version of the manuscript. Y.Y., Z.X., and J.G.C. conceived the idea and designed the experiments; Y.Y. and Z.X. carried out catalyst synthesis; Y.Y. performed the catalyst characterizations, including TEM measurements, H₂-TPR, and pulse CO-chemisorption; Z.X. established the reactor system and methodology, conducted the XAFS measurements and analysis, and contributed to the initial draft; J.Z. performed the BET and XRF measurements; S.H. performed the HAADF-STEM images and EDS elemental maps; K.K.T. participated in the discussion and contributed to part of the introduction section; Y.Y. prepared the initial draft; Y.Y, Z.X., K.K.T., and J.G.C reviewed and edited the paper; J.G.C. supervised the whole project.

Notes

The authors declare no competing financial interest.

■ ACKNOWLEDGMENTS

This work was supported by the US Department of Energy (DOE), Office of Science, Office of Basic Energy Sciences (BES), Division of Chemical Sciences, Geosciences and

Biosciences through a subcontract from PNNL (FWP 78459). This research used resources at the Center for Functional Nanomaterials (CFN) and beamline 7-BM (QAS) of the National Synchrotron Light Source II (NSLS-II) at Brookhaven National Laboratory (Contract Nos. DE-SC0012704 and DE-SC0012653). Beamline operations were supported in part by the Synchrotron Catalysis Consortium (U.S. DOE, Office of Basic Energy Sciences, Grant No. DE-SC0012335).

■ REFERENCES

- (1) Hu, H.; Chen, Y.; You, F.; Yao, J.; Yang, H.; Jiang, X.; Xia, B. Y. Recycling and Upgrading Utilization of Polymer Plastics†. *Chin. J. Chem.* **2023**, *41*, 469–480.
- (2) Yang, R.-X.; Jan, K.; Chen, C.-T.; Chen, W.-T.; Wu, K. C.-W. Thermochemical Conversion of Plastic Waste into Fuels, Chemicals, and Value-Added Materials: A Critical Review and Outlooks. *ChemSusChem* **2022**, *15*, No. e202200171.
- (3) Geyer, R.; Jambeck, J. R.; Law, K. L. Production, Use, and Fate of All Plastics Ever Made. *Sci. Adv.* **2017**, *3*, No. e1700782.
- (4) Vollmer, I.; Jenks, M. J. F.; Roelands, M. C. P.; White, R. J.; van Harmelen, T.; de Wild, P.; van der Laan, G. P.; Meirer, F.; Keurentjes, J. T. F.; Weckhuysen, B. M. Beyond Mechanical Recycling: Giving New Life to Plastic Waste. *Angew. Chem. Int. Ed.* **2020**, *59*, 15402–15423.
- (5) Jawaid, M.; Singh, B.; Kian, L. K.; Zaki, S. A.; Radzi, A. M. Processing Techniques on Plastic Waste Materials for Construction and Building Applications. *Curr. Opin. Green Sustain. Chem.* **2023**, *40*, 100761.
- (6) Ragaert, K.; Delva, L.; Van Geem, K. Mechanical and Chemical Recycling of Solid Plastic Waste. *Waste Manage.* **2017**, *69*, 24–58.
- (7) Roy, P. S.; Garnier, G.; Allais, F.; Saito, K. Strategic Approach Towards Plastic Waste Valorization: Challenges and Promising Chemical Upcycling Possibilities. *ChemSusChem* **2021**, *14*, 4007–4027.
- (8) Chen, X.; Wang, Y.; Zhang, L. Recent Progress in the Chemical Upcycling of Plastic Wastes. *ChemSusChem* **2021**, *14*, 4137–4151.
- (9) Martín, A. J.; Mondelli, C.; Jaydev, S. D.; Perez-Ramirez, J. Catalytic Processing of Plastic Waste on the Rise. *Chem.* **2021**, *7*, 1487–1533.
- (10) Wei, J.; Liu, J.; Zeng, W.; Dong, Z.; Song, J.; Liu, S.; Liu, G. Catalytic Hydroconversion Processes for Upcycling Plastic Waste to Fuels and Chemicals. *Catal. Sci. Technol.* **2023**, *13*, 1258–1280.
- (11) Kots, P. A.; Vance, B. C.; Vlachos, D. G. Polyolefin Plastic Waste Hydroconversion to Fuels, Lubricants, and Waxes: A Comparative Study. *React. Chem. Eng.* **2022**, *7*, 41–54.
- (12) Kots, P. A.; Liu, S.; Vance, B. C.; Wang, C.; Sheehan, J. D.; Vlachos, D. G. Polypropylene Plastic Waste Conversion to Lubricants over Ru/TiO₂ Catalysts. *ACS Catal.* **2021**, *11*, 8104–8115.
- (13) Chen, L.; Meyer, L. C.; Kovarik, L.; Meira, D.; Pereira-Hernandez, X. I.; Shi, H.; Khivantsev, K.; Gutiérrez, O. Y.; Szanyi, J. Disordered, Sub-Nanometer Ru Structures on CeO₂ Are Highly Efficient and Selective Catalysts in Polymer Upcycling by Hydrogenolysis. *ACS Catal.* **2022**, *12*, 4618–4627.
- (14) Galadima, A.; Masudi, A.; Muraza, O. Towards Low-Temperature Catalysts for Sustainable Fuel from Plastic: A Review. *J. Environ. Chem. Eng.* **2021**, *9*, 106655.
- (15) Sinfelt, J. H. Specificity in Catalytic Hydrogenolysis by Metals. *Adv. Catal.* **1973**, *23*, 91–119.
- (16) Celik, G.; Kennedy, R. M.; Hackler, R. A.; Ferrandon, M.; Tennakoon, A.; Patnaik, S.; LaPointe, A. M.; Ammal, S. C.; Heyden, A.; Perras, F. A.; Pruski, M.; Scott, S. L.; Poepelmeier, K. R.; Sadow, A. D.; Delferro, M. Upcycling Single-Use Polyethylene into High-Quality Liquid Products. *ACS Cent. Sci.* **2019**, *5*, 1795–1803.
- (17) Zhang, F.; Zeng, M.; Yappert, R. D.; Sun, J.; Lee, Y.-H.; LaPointe, A. M.; Peters, B.; Abu-Omar, M. M.; Scott, S. L. Polyethylene Upcycling to Long-Chain Alkylaromatics by Tandem Hydrogenolysis/Aromatization. *Science* **2020**, *370*, 437–441.

- (18) Tennakoon, A.; Wu, X.; Paterson, A. L.; Patnaik, S.; Pei, Y.; LaPointe, A. M.; Ammal, S. C.; Hackler, R. A.; Heyden, A.; Slowing, I. I.; Coates, G. W.; Delferro, M.; Peters, B.; Huang, W.; Sadow, A. D.; Perras, F. A. Catalytic Upcycling of High-Density Polyethylene via a Processive Mechanism. *Nat. Catal.* **2020**, *3*, 893–901.
- (19) Liu, S.; Kots, P. A.; Vance, B. C.; Danielson, A.; Vlachos, D. G. Plastic Waste to Fuels by Hydrocracking at Mild Conditions. *Sci. Adv.* **2021**, *7*, No. eabf8283.
- (20) Jia, C.; Xie, S.; Zhang, W.; Intan, N. N.; Sampath, J.; Pfaendtner, J.; Lin, H. Deconstruction of High-Density Polyethylene into Liquid Hydrocarbon Fuels and Lubricants by Hydrogenolysis over Ru Catalyst. *Chem. Catal.* **2021**, *1*, 437–455.
- (21) Rorrer, J. E.; Beckham, G. T.; Román-Leshkov, Y. Conversion of Polyolefin Waste to Liquid Alkanes with Ru-Based Catalysts under Mild Conditions. *JACS Au* **2021**, *1*, 8–12.
- (22) Chen, L.; Zhu, Y.; Meyer, L. C.; Hale, L. V.; Le, T. T.; Karkamkar, A.; Lercher, J. A.; Gutiérrez, O. Y.; Szanyi, J. Effect of Reaction Conditions on the Hydrogenolysis of Polypropylene and Polyethylene into Gas and Liquid Alkanes. *React. Chem. Eng.* **2022**, *7*, 844–854.
- (23) Rorrer, J. E.; Troyano-Valls, C.; Beckham, G. T.; Román-Leshkov, Y. Hydrogenolysis of Polypropylene and Mixed Polyolefin Plastic Waste over Ru/C to Produce Liquid Alkanes. *ACS Sustain. Chem. Eng.* **2021**, *9*, 11661–11666.
- (24) Kots, P. A.; Xie, T.; Vance, B. C.; Quinn, C. M.; de Mello, M. D.; Boscoboinik, J. A.; Wang, C.; Kumar, P.; Stach, E. A.; Marinkovic, N. S.; Ma, L.; Ehrlich, S. N.; Vlachos, D. G. Electronic Modulation of Metal-Support Interactions Improves Polypropylene Hydrogenolysis over Ruthenium Catalysts. *Nat. Commun.* **2022**, *13*, 5186.
- (25) Lee, S.; Shen, K.; Wang, C.-Y.; Vohs, J. M.; Gorte, R. J. Hydrogenolysis of N-Eicosane over Ru-Based Catalysts in a Continuous Flow Reactor. *Chem. Eng. J.* **2023**, *456*, 141030.
- (26) Wang, C.; Xie, T.; Kots, P. A.; Vance, B. C.; Yu, K.; Kumar, P.; Fu, J.; Liu, S.; Tsilomelekis, G.; Stach, E. A.; Zheng, W.; Vlachos, D. G. Polyethylene Hydrogenolysis at Mild Conditions over Ruthenium on Tungstated Zirconia. *JACS Au* **2021**, *1*, 1422–1434.
- (27) Wang, C.; Yu, K.; Sheludko, B.; Xie, T.; Kots, P. A.; Vance, B. C.; Kumar, P.; Stach, E. A.; Zheng, W.; Vlachos, D. G. A General Strategy and a Consolidated Mechanism for Low-Methane Hydrogenolysis of Polyethylene over Ruthenium. *Appl. Catal. B: Environ.* **2022**, *319*, 121899.
- (28) Mohammed, A. A.; Olabemiwo, O. M.; Olajire, A. A. Green Synthesized Pd-Ni Nanohybrids for Controlled Degradation of Low-Density Polyethylene Films. *Chem. Eng. Commun.* **2023**, *210* (11), 2043–2056.
- (29) Hagggar, A. M.; Awadallah, A. E.; Aboul-Enein, A. A.; Sayed, G. H. Non-Oxidative Conversion of Real Low Density Polyethylene Waste into Hydrogen and Carbon Nanomaterials over MgO Supported Bimetallic Co-Mo Catalysts with Different Total Co-Mo Contents. *Chem. Eng. Sci.* **2022**, *247*, 117092.
- (30) Chen, Z.; Xu, L.; Zhang, X. Upgrading of Polyethylene to Hydrocarbon Fuels over the Fe-Modified Pt/Al₂O₃ Catalysts at a Mild Condition without External H₂. *Chem. Eng. J.* **2022**, *446*, 136213.
- (31) Nakaji, Y.; Nakagawa, Y.; Tamura, M.; Tomishige, K. Regioselective Hydrogenolysis of Alga-Derived Squalane over Silica-Supported Ruthenium-Vanadium Catalyst. *Fuel Process. Technol.* **2018**, *176*, 249–257.
- (32) Lu, S.; Jing, Y.; Jia, S.; Shakouri, M.; Hu, Y.; Liu, X.; Guo, Y.; Wang, Y. Enhanced Production of Liquid Alkanes from Waste Polyethylene via the Electronic Effect-Favored C_{secondary}-C_{secondary} Bond Cleavage. *ChemCatChem* **2023**, *15* (3), No. e202201375.
- (33) Chu, M.; Wang, X.; Wang, X.; Lou, X.; Zhang, C.; Cao, M.; Wang, L.; Li, Y.; Liu, S.; Sham, T.-K.; Zhang, Q.; Chen, J. Site-Selective Polyolefin Hydrogenolysis on Atomic Ru for Methanation Suppression and Liquid Fuel Production. *Research* **2023**, *6*, 0032.
- (34) Wu, X.; Tennakoon, A.; Yappert, R.; Esveld, M.; Ferrandon, M. S.; Hackler, R. A.; LaPointe, A. M.; Heyden, A.; Delferro, M.; Peters, B.; Sadow, A. D.; Huang, W. Size-Controlled Nanoparticles Embedded in a Mesoporous Architecture Leading to Efficient and Selective Hydrogenolysis of Polyolefins. *J. Am. Chem. Soc.* **2022**, *144*, 5323–5334.
- (35) Xie, Z.; Xu, Y.; Xie, M.; Chen, X.; Lee, J. H.; Stavitski, E.; Kattel, S.; Chen, J. G. Reactions of CO₂ and Ethane Enable CO Bond Insertion for Production of C₃ Oxygenates. *Nat. Commun.* **2020**, *11*, 1887.
- (36) Ravel, B.; Newville, M. ATHENA, ARTEMIS, HEPHAESTUS: Data Analysis for X-Ray Absorption Spectroscopy Using IFEFFIT. *J. Synchrotron Radiat.* **2005**, *12*, 537–541.
- (37) Nakaji, Y.; Tamura, M.; Miyaoka, S.; Kumagai, S.; Tanji, M.; Nakagawa, Y.; Yoshioka, T.; Tomishige, K. Low-Temperature Catalytic Upgrading of Waste Polyolefinic Plastics into Liquid Fuels and Waxes. *Appl. Catal. B: Environ.* **2021**, *285*, 119805.
- (38) Xiang, L.; Fan, G.; Yang, L.; Zheng, L.; Li, F. Structure-Tunable Pompon-like RuCo Catalysts: Insight into the Roles of Atomically Dispersed Ru-Co Sites and Crystallographic Structures for Guaiacol Hydrodeoxygenation. *J. Catal.* **2021**, *398*, 76–88.
- (39) Liu, W.; Feng, H.; Yang, Y.; Niu, Y.; Wang, L.; Yin, P.; Hong, S.; Zhang, B.; Zhang, X.; Wei, M. Highly-Efficient RuNi Single-Atom Alloy Catalysts toward Chemoselective Hydrogenation of Nitroarenes. *Nat. Commun.* **2022**, *13*, 3188.
- (40) Rui, N.; Zhang, X.; Zhang, F.; Liu, Z.; Cao, X.; Xie, Z.; Zou, R.; Senanayake, S. D.; Yang, Y.; Rodriguez, J. A.; Liu, C.-J. Highly Active Ni/CeO₂ Catalyst for CO₂ Methanation: Preparation and Characterization. *Appl. Catal. B: Environ.* **2021**, *282*, 119581.
- (41) Liu, Z.; Li, J.; Wang, R. CeO₂ Nanorods Supported M-Co Bimetallic Oxides (M = Fe, Ni, Cu) for Catalytic CO and C₃H₈ Oxidation. *J. Colloid Interface Sci.* **2020**, *560*, 91–102.
- (42) Wang, F.; Li, C.; Zhang, X.; Wei, M.; Evans, D. G.; Duan, X. Catalytic Behavior of Supported Ru Nanoparticles on the {100}, {110}, and {111} Facet of CeO₂. *J. Catal.* **2015**, *329*, 177–186.
- (43) Chen, J. G.; Menning, C. A.; Zellner, M. B. Monolayer Bimetallic Surfaces: Experimental and Theoretical Studies of Trends in Electronic and Chemical Properties. *Surf. Sci. Rep.* **2008**, *63*, 201–254.